Optimization of flow distribution by topological description and machine learning in solution growth of SiC

Masaru Isono, Shunta Harada*, Kentaro Kutsukake, Tomoo Yokoyama, Miho Tagawa, Toru Ujihara

M. Isono, S. Harada, M. Tagawa, T. Ujihara
Department of Materials Process Engineering, Nagoya University, Furo-cho, Chikusa-ku, Nagoya 464-8603, Japan
E-mail: shunta.harada@nagoya-u.jp

S. Harada, M. Tagawa, T. Ujihara
Institute of Materials and Systems for Sustainability (IMaSS), Nagoya University, Furo-cho, Chikusa-ku, Nagoya 464-8601, Japan

K. Kutsukake
Center for Advanced Intelligence Project, RIKEN, Nihonbashi, Chuo-ku, Tokyo 103-0027, Japan

T. Yokoyama
Applied Mathematics and Physics Division, Gifu University, Yanagido 1-1, Gifu 501-1193, Japan
Keywords: topology, machine learning, crystal growth, SiC

The macroscopic distribution of fluid flows, which affect the quality of final products for various kinds of materials, is often difficult to describe in mathematical formulae, and hinders the implementation of empirical knowledge in scaling up. In the present study, we described the characteristics of the flow distribution in SiC solution growth by using the position of the saddle point and optimized the solution growth conditions by computational fluid dynamics simulation, machine learning and a genetic algorithm. As a result, we successfully obtained the candidates of the optimal condition for the solution growth of 6-inch SiC crystals from the empirical knowledge gained from 3-inch crystal growth, by adding the topological description to the objective function. The present design of the objective function using the topological description can possibly be applied to other crystal growth or materials processing problems

and to overcome scale-up difficulties, which can facilitate the rapid development of functional materials such as SiC wafers for power device applications.

1. Introduction

Fluid flow that arises in many materials processing techniques, such as crystal growth, casting, thin film fabrication, and polymer processing, is critical to the quality and characteristics of the final product and optimization of the system[1]. Recent advances in computational fluid dynamics (CFD) aid in the design of suitable conditions for materials processing[2]. Furthermore, the application of machine learning techniques to CFD simulations greatly reduces the calculation time, so that it is possible to efficiently optimize the conditions for materials processing[3–9]. For mathematical optimization of the conditions for materials processing, it is necessary to define the objective function representing the optimal conditions to achieve high-quality products. In most cases, local values near or on the boundary between the material and fluid areas, such as the flow vectors, temperature, and crystal growth rate, are used as the objective function and optimized. However, not only such local property values but also the global flow distribution often determine the quality of final products. For example, in the solution growth of silicon carbide (SiC), which is a promising method to obtain high-quality crystals for high-power devices[10–15], the crystal quality and crystal growth rate largely depend on the global flow distribution, since the global flow affects the transport of solute atoms, long-term growth stability and the attachment of polycrystals crystalized at the bottom of the crucible or in solution on the grown surface [12,16–24]. However, as is the case with the processing of other materials, the optimal global flow distribution is difficult to define. In the field of mathematics, the characteristic features of vector fields are extracted, visualized, and classified by topology. In the present study, we optimized the global flow distribution during solution growth of 6-inch SiC crystals from the knowledge gained from smaller size (3-inch) crystal growth by means of topological description as well as machine learning.

2. Topological description of flow

In topological analysis of a vector field, a stagnation point where the flow is zero in a vector field is important. **Figure 1** shows stagnation points that occur in a two-dimensional conservative vector field. A stagnation point around which the flow is swirling as shown in Fig. 1(a) is called a center point, while a stagnation point where the incoming flow is deflected and directed in a different direction as shown in Fig. 1(b) is called a saddle point[25].

Although the flow velocities at these two points were zero, we can identify from the calculation of the index of a vector field. The index of a vector field is an integer that describes the character of a stagnation point. The index I_C of the closed loop C in the two-dimensional vector field $\boldsymbol{f}(x,y)$ is defined as follows[25]:

$$I_C = \frac{1}{2\pi}[\phi]_C \quad (1)$$

where ϕ is the angle between the vector f on C and the x axis, and $[\phi]_C$ represents the total change in ϕ while going around C. Note that the index I_C is independent of the path of the closed loop C. To calculate the index, it is not necessary to know the vector field at all points, only at several points on C. Fig. 1(c) and 1(d) show an example of the calculation of the index. When the closed curve C is rotated once counterclockwise as in Fig. 1(c), the vector on C rotates clockwise. As shown in Fig. 1(d), the vector rotates clockwise from 1 to 8 and the index can be calculated as -1. Since the indexes of the center and saddle points are 1 and -1, the stagnation points can be distinguished by calculation of the index.

3. Method

3.1. CFD simulation

Figure 2 shows a schematic illustration of the 6-inch SiC solution growth furnace. In top-seeded solution growth (TSSG) of SiC, a Si-based solvent is melted in a carbon crucible. More details on the TSSG setup are found in the literature[5,6,26]. The CFD simulation was performed on a 2D steady axisymmetric model by taking account of the heat transport, mass transport, and convection using CGSim software[27]. The temperatures inside the seed shaft (T), the rotation speeds of the seed shaft (ω_s) and crucible (ω_c) and the position of the crucible (z) were set as variable parameters.

3.2. Machine learning

For rapid optimization of the 6-inch TSSG condition, we constructed a machine learning model to predict the results of CFD simulation from the variable parameters using a neural network (NN), as previously reported[4]. We prepared 490 CFD simulations with different values for the variable parameters. The values were randomly selected from the ranges shown in **Table 1**, which were determined based on actual growth experiments. The 490 datasets were divided into training (397), validation (44) and testing (49) datasets. The former two datasets were used for training of the NN model, while the testing dataset was used for evaluation of the trained NN model. **Figure 3** shows the structure of NN. In addition to the 4 variable parameters (T_0, ω_s, ω_c and z), the coordinate positions in the solvent (r, y)

were used as input parameters. Thus, this NN model predicts the temperature (T) and velocities of horizontal and vertical flows (v_h, v_v) from the TSSG conditions and the position in the solvent. The number of hidden layers is 2 and the number of nodes for each hidden layer is 128. Rectified linear unit (ReLU) was used as the activation function. The NN was optimized by adaptive moment estimation (Adam) using TensorFlow[28]. **Figure 4** shows parity plots of the temperature distribution, horizontal flow velocity distribution, and vertical flow velocity distribution for the test data as well as the predicted distributions of temperature and fluid flow. The plot points are concentrated on the straight red line. As shown in Figs. 4(d) and 4(e), the distribution of temperature and solution flow was well-reconstructed by the trained NN model. **Table 2** summarizes the coefficients of determination (R^2) and average root mean square error (RMSE) for the prediction values of temperature, horizontal flow velocity, and vertical flow velocity. The values of RMSE for flow speed are enough low compared to the typical range of flow speed for horizontal direction (-100 ~ 200 mm/s) and vertical direction (-100 ~ 50 mm/s). These results indicate that the trained NN model was sufficiently precise to search for the optimal crystal growth conditions. While CFD simulation requires about 10 h, the prediction by the trained NN could calculate the distributions within 1 s with Intel® Core™ i5-8365UE CPU, enabling us to mathematically optimize the crystal growth conditions within a feasible calculation time with high precision.

3.3. Extraction of stagnation points

From the flow velocity distribution $\boldsymbol{v}(r, y)$ calculated as 2-dimensional data grid, we extracted stagnation points by the calculation of the index for 8-neibour. **Figure 5** shows a schematic illustration of the index calculation for flow velocity at point A. To judge whether point A is a stagnation point or not, the index at point A is calculated by Eq. (1) with the square connecting the 8 neighbors of point A as a closed curve C. By repeating this calculation at each point in the solvent, stagnation points were extracted, including center points (I_C = 1) and saddle points (I_C = -1). On the boundary, the index was calculated by creating a mirror image of the flow distribution at the boundary. By this operation, boundary saddle points can be extracted. A program was made to automatically determine stagnation points by calculating the index for each mesh point in the solution. **Figure 6** shows the result of the extraction of stagnation points in the CFD simulation result as one example. Center, saddle and boundary saddle points were successfully extracted with calculation times of less than 0.1 second with Intel® Core™ i5-8365UE CPU. The extracted stagnation points were

used to calculate the objective function for the macroscopic flow distribution as described in the next section.

3.4. Mathematical optimization

A genetic algorithm (GA) was applied as the mathematical optimization method to determine the optimal variable parameters for the 6-inch TSSG condition. GA is a parallel iterative searching algorithm that is inspired by the idea of "survival of the fittest" and "natural selection" from evolution theory, which repeats evaluation, selection, crossover, and mutation after initialization until the stopping condition is satisfied[29,30]. Multi-objective optimization of the objective functions described in the next section was performed using NSGA-II[31], a high-speed non-dominated sorting algorithm. The population size and termination criteria were set to 1000 and 100, respectively. The multi-objective optimization cannot produce a perfect solution of the incommensurability between different objectives. A series of Pareto-optimal solutions, which shows the trade-off relationship between objectives, were produced by GA[32].

4. Design of objective functions for 6-inch SiC crystal growth

Since solution growth of SiC has advantages in obtaining high-quality bulk crystals using dislocation conversion [10,11,14,15,33–37], many researchers have reported the bulk crystal growth of SiC, especially by the TSSG method [12,13,38–43]. Recently, crystal growth of SiC wafers with a diameter of 4 inches and a thickness of 20 mm has been reported[44] and the possibility of growing larger SiC crystals by TSSG was investigated[5]. As is the case with other materials processing operations, scaling-up always encounters difficulties, and in some cases the empirical knowledge gained from manufacturing small products cannot be transferred directly to a process for larger products. In our study on TSSG of 3-inch SiC wafers combining actual experiments and CFD simulations, we found the homogeneous temperature distribution in the solution to suppress unintentional precipitation of crystals on the crucible and the crystal, and the homogeneous horizontal component of solution flow on the crystal to maintain a smooth growth surface by the switching flow method[37,45], which are defined as objective functions F_1 and F_2 as follows;

$$F_1 = \max_{\text{in solution}}\big(T(r,y)\big) - \min_{\text{in solution}}\big(T(r,y)\big), \qquad (2)$$

$$F_2 = \max_{\text{on crystal}}\big(v_h(r,y)\big) - \min_{\text{on crystal}}\big(v_h(r,y)\big). \qquad (3)$$

These two objective functions should be minimized and can be calculated from the results predicted by the trained NN. In addition, we noticed in our experiments of 3-inch SiC growth that the global flow distribution shown in **Figure 7**, in which two vortexes are separated at the top and bottom, is favorable for stable crystal growth. However, unlike the former two situation, the current situation is difficult to represent as mathematical descriptions for the optimization of 6-inch SiC crystal growth conditions since the characteristic feature is not described by the local values as F_1 and F_2 but the global distribution of solution flow. Therefore, here we utilized the topological description to represent the desired flow conditions as mathematical formulae.

For the achievement of the two vortexes separated at the top and bottom, two saddle points should exist in the center of the solution ($r = 0$) and on the crucible wall ($r = r_c$), which makes a heteroclinic connection. It seems that it is no preferential position (y) of these two boundary saddle points as long as two vortexes separated at the top and bottom. Thus, we set the referent points (P and Q) at the middle of the solution ($y = 0.5d_s$), and defined the objective function F_3 as follows:

$$F_3 = min(|\overline{S_k P}|) + min(|\overline{S_k Q}|), \quad (4)$$

where S_k are the saddle points in the solution and P and Q are the referent saddle points. $|\overline{S_k P}|$ and $|\overline{S_k Q}|$ stand for the distances between the kth saddle point and P and Q. The objective function F_3 is the sum of the distances between the saddle point and the coordinates of the referent point. Here, the coordinates of the referent saddle point as (r, y) = P(0, $0.5d_s$) and Q(r_c, $0.5d_s$). If there is no saddle point, we assign F_3 a large value ($F_3 = 1000$). Calculation of the objective function F_3 during optimization was possible from the results predicted by the trained NN and the algorithm for the extraction of stagnation points.

5. Results of optimization

Figure 8 shows the pareto front for the three objective functions F_1, F_2 and F_3 as well as the distributions of temperature and solution flow velocity for 6-inch SiC crystal growth with the selected optimal solutions, which indicates a trade-off relationship between the 3 objective functions. Among the pareto solutions, Solution-(A) is a solution with a small value of F_3, solution-(B) is a solution with a moderate value of F_3, and solution-(C) is a solution with a large value of F_3. The values of the objective functions and the parameters of the crystal growth conditions are tabulated in **Table 3**. The larger the value of F_3 is, the more greatly saddle points deviate from the referent saddle points. Note that most of the solutions satisfy the desired conditions in which the solution flow is separated at the top and bottom,

although a few solutions did not seem to be satisfactory, as shown for solution-(D), in which the number of vortexes is different and complex solution flow is formed near the center of the crucible. This indicates that the objective function F_3 is a good description of the desired condition.

To verify the effectiveness of adding the objective function F_3 which topologically describes the desired global flow distribution, we conducted multi-objective optimization without the objective function F_3. **Figure 9** shows the pareto front for the two objective functions F_1 and F_2 as well as the three objective functions with a value of F_3 of less than 10. Although some solutions seem to occasionally satisfy the desired conditions, most of the pareto solutions have a quite different distribution of fluid flow in which the number and the configuration of vortexes are different, as shown for solution-(E).

Among the pareto solutions for the three objective functions F_1, F_2 and F_3 with relatively small values of F_3 (<10), we found two types of distributions for the solution. In one, the lower vortex is pushed by the upper vortex as shown in Fig. 8 (solution-(A)), and in the other the boundary line between the upper and lower vortex is linear as shown in Fig. 9 (solution-(E)). Since the former type of distribution may result in the transportation of the precipitated crystals on the bottom of the crucible to the grown crystal, the latter type, in which precipitated crystals tends to be confined by the bottom vortex, was determined to be preferable. As a result, we have successfully obtained the candidate of optimal crystal growth condition as solution-(F).

In the present study, we successfully obtained the candidates of optimal condition for solution growth of 6-inch SiC wafers from the empirical knowledge gained from smaller size (3-inch) crystal growth by using the topological description of the objective function. The present design of the objective function using the topological description can possibly be applied to other crystal growth or materials processing systems to overcome difficulties in scaling-up, which can lead to the rapid development of functional materials, such as SiC wafers for power device applications.

5. Summary

We optimized the solution flow distribution during solution growth of SiC crystal with the diameter of 6 inch based on the knowledge gained from 3-inch growth by using the objective function designed by the topological description. A machine learning model that can rapidly and precisely predict the temperature and fluid flow distributions in solution from a set of input variables for crystal growth conditions was constructed from the training dataset of CFD

simulations using neural networks. Saddle points in the solution were successfully extracted from the predicted fluid flow distribution followed by the application of index theory. The objective functions were designed considering the global flow distribution, in which two vortexes are separated at the top and bottom by the distances between the coordinates of the saddle point and referent points. After multi-purpose optimization of the designed objective function, we successfully obtained crystal growth conditions that can realize the desired flow distribution. The present results indicate that the optimization of the objective function represented by topological description of fluid flow can enable us to overcome the difficulties faced in scaling-up and lead to the rapid development of functional materials, such as SiC grown by solution growth.

Acknowledgements

This paper is based on results obtained from a project JPNP20006 commissioned by the New Energy and Industrial Technology Development Organization (NEDO).

Received: ((will be filled in by the editorial staff))

Revised: ((will be filled in by the editorial staff))

Published online: ((will be filled in by the editorial staff))

References

[1] Y. Jaluria, *Journal of Fluids Engineering* **2001**, *123*, 173.
[2] J. F. Wendt, J. D. Anderson, J. Degroote, G. Degrez, E. Dick, R. Grundmann, J. Vierendeels, *Computational Fluid Dynamics: An Introduction*, Springer Berlin Heidelberg, **2009**.
[3] D. Kochkov, J. A. Smith, A. Alieva, Q. Wang, M. P. Brenner, S. Hoyer, *Proceedings of the National Academy of Sciences* **2021**, *118*.
[4] Y. Tsunooka, N. Kokubo, G. Hatasa, S. Harada, M. Tagawa, T. Ujihara, *CrystEngComm* **2018**, *20*.
[5] W. Yu, C. Zhu, Y. Tsunooka, H. Wei, D. Yifan, K. Kentaro, H. Shunta, T. Miho, U. Toru, *CrystEngComm* **2021**, *23*, 2695.
[6] Y. Dang, C. Zhu, M. Ikumi, M. Takaishi, W. Yu, W. Huang, X. Liu, K. Kutsukake, S. Harada, M. Tagawa, T. Ujihara, *CrystEngComm* **2021**, *23*, 1982.
[7] N. Dropka, M. Holena, S. Ecklebe, C. Frank-Rotsch, J. Winkler, *Journal of Crystal Growth* **2019**, *521*, 9.
[8] N. Dropka, M. Holena, *Journal of Crystal Growth* **2017**, *471*, 53.
[9] L. Wang, A. Sekimoto, Y. Takehara, Y. Okano, T. Ujihara, S. Dost, *Crystals (Basel)* **2020**, *10*, 791.
[10] Y. Yamamoto, S. Harada, K. Seki, A. Horio, T. Mitsuhashi, T. Ujihara, *Applied Physics Express* **2012**, *5*, 115501.
[11] Y. Yamamoto, S. Harada, K. Seki, A. Horio, T. Mitsuhashi, D. Koike, M. Tagawa, T. Ujihara, *Applied Physics Express* **2014**, *7*, 065501.
[12] K. Kusunoki, N. Okada, K. Kamei, K. Moriguchi, H. Daikoku, M. Kado, H. Sakamoto, T. Bessho, T. Ujihara, *Journal of Crystal Growth* **2014**, *395*, 68.

[13] H. Daikoku, M. Kado, A. Seki, K. Sato, T. Bessho, K. Kusunoki, H. Kaidou, Y. Kishida, K. Moriguchi, K. Kamei, *Crystal Growth & Design* **2016**, *16*, 1256.
[14] T. Mitani, K. Eto, N. Komatsu, Y. Hayashi, H. Suo, T. Kato, *Journal of Crystal Growth* **2021**, 126189.
[15] T. Mitani, K. Eto, K. Momose, T. Kato, *Applied Physics Express* **2021**, *14*, 085506.
[16] T. Yamamoto, Y. Okano, T. Ujihara, S. Dost, *Journal of Crystal Growth* **2017**, *470*, 75.
[17] T. Yamamoto, N. Adkar, Y. Okano, T. Ujihara, S. Dost, *Journal of Crystal Growth* **2017**, *474*, 50.
[18] S. Harada, Alexander, K. Seki, Y. Yamamoto, C. Zhu, Y. Yamamoto, S. Arai, J. Yamasaki, N. Tanaka, T. Ujihara, *Crystal Growth & Design* **2012**, *12*, 3209.
[19] T. Umezaki, D. Koike, S. Harada, T. Ujihara, *Japanese Journal of Applied Physics* **2016**, *55*, 125601.
[20] M. T. Ha, Y. J. Shin, S. Y. Bae, S. Y. Park, S. M. Jeong, *Journal of the Korean Ceramic Society* **2019**, *56*, 589.
[21] M. T. Ha, Y. J. Shin, M. H. Lee, C. J. Kim, S. M. Jeong, *physica status solidi (a)* **2018**, *215*, 1701017.
[22] M. T. Ha, Y. J. Yu, Y. J. Shin, S. Y. Bae, M. H. Lee, C. J. Kim, S. M. Jeong, *RSC Advances* **2019**, *9*, 26327.
[23] K. Ariyawong, Y. J. Shin, J. M. Dedulle, D. Chaussende, *Crystal Growth and Design* **2016**, *16*, 3231.
[24] B. Liu, Y. Yu, X. Tang, B. Gao, *Journal of Crystal Growth* **2019**, *527*, 125248.
[25] G. Hector, U. Hirsch, *Introduction to the Geometry of Foliation, Part B* **1983**, DOI 10.1007/978-3-322-85619-7.
[26] Y. Dang, C. Zhu, X. Liu, W. Yu, X. Liu, K. Suzuki, T. Furusho, S. Harada, M. Tagawa, T. Ujihara, *Journal of Crystal Growth* **2022**, *579*, 126448.
[27] Y. Mukaiyama, M. Iizuka, A. Vorob'ev, V. Kalaev, *Journal of Crystal Growth* **2017**, *475*, 178.
[28] "TensorFlow," can be found under https://www.tensorflow.org/, **2022**.
[29] L. Wang, *Applied Mathematics and Computation* **2005**, *170*, 1329.
[30] J. Horn, N. Nafpliotis, D. E. Goldberg, *IEEE Conference on Evolutionary Computation - Proceedings* **1994**, *1*, 82.
[31] K. Deb, A. Pratap, S. Agarwal, T. Meyarivan, *IEEE Transactions on Evolutionary Computation* **2002**, *6*, 182.
[32] P. Ngatchou, A. Zarei, M. A. El-Sharkawi, *Proceedings of the 13th International Conference on Intelligent Systems Application to Power Systems, ISAP'05* **2005**, *2005*, 84.
[33] S. Harada, Y. Yamamoto, K. Seki, A. Horio, T. Mitsuhashi, M. Tagawa, T. Ujihara, *APL Materials* **2013**, *1*, 022109.
[34] S. Harada, Y. Yamamoto, K. Seki, A. Horio, M. Tagawa, T. Ujihara, *Acta Materialia* **2014**, *81*, 284.
[35] S. Harada, Y. Yamamoto, S. Xiao, D. Koike, T. Mutoh, K. Murayama, K. Aoyagi, T. Sakai, M. Tagawa, T. Ujihara, *Materials Science Forum* **2015**, *821–823*, 3.
[36] S. Xiao, S. Harada, K. Murayama, M. Tagawa, T. Ujihara, *Crystal Growth and Design* **2016**, *16*, 6436.
[37] X. Liu, C. Zhu, S. Harada, M. Tagawa, T. Ujihara, *CrystEngComm* **2019**, *21*, 7260.
[38] T. Mitani, N. Komatsu, T. Takahashi, T. Kato, S. Harada, T. Ujihara, Y. Matsumoto, K. Kurashige, H. Okumura, *Journal of Crystal Growth* **2015**, *423*, 45.
[39] K. Nakano, S. Maruyama, T. Kato, Y. Yonezawa, H. Okumura, Y. Matsumoto, *Surfaces and Interfaces* **2022**, *28*, 101664.

[40] S. Kawanishi, H. Daikoku, H. Shibata, T. Yoshikawa, *Journal of Crystal Growth* **2021**, *576*, 126382.
[41] S. Kawanishi, Y. Nagamatsu, T. Yoshikawa, H. Shibata, *Journal of Crystal Growth* **2020**, *549*, 125877.
[42] X. Xing, T. Yoshikawa, O. Budenkova, D. Chaussende, *Journal of Materials Science* **2022**, *57*, 972.
[43] H. Daikoku, S. Kawanishi, T. Yoshikawa, *Crystal Growth and Design* **2018**, *18*, 3820.
[44] K. Kusunoki, Y. Kishada, K. Seki, *Materials Science Forum* **2019**, *963*, 85.
[45] C. Zhu, S. Harada, K. Seki, H. Zhang, H. Niinomi, M. Tagawa, T. Ujihara, *Crystal Growth & Design* **2013**, *13*, 3691.

M. Isono, S. Harada*, K. Kutsukake, T. Yokoyama, M. Tagawa, T. Ujihara

Optimization of flow distribution by topological description and machine learning in SiC solution growth

ToC

Application of the topological description of fluid flow to the design of the objective function for the optimization of the material process enables us to implement the empirical knowledge gained from small size production in scaling up crystal growth. We successfully find the optimal conditions for the solution growth of 6-inch SiC wafers from the empirical knowledge gained from 3-inch wafer growth by using CFD simulation, machine learning and mathematical optimization.

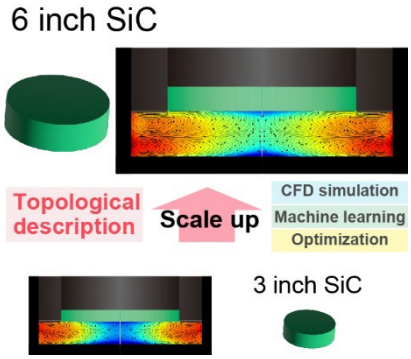

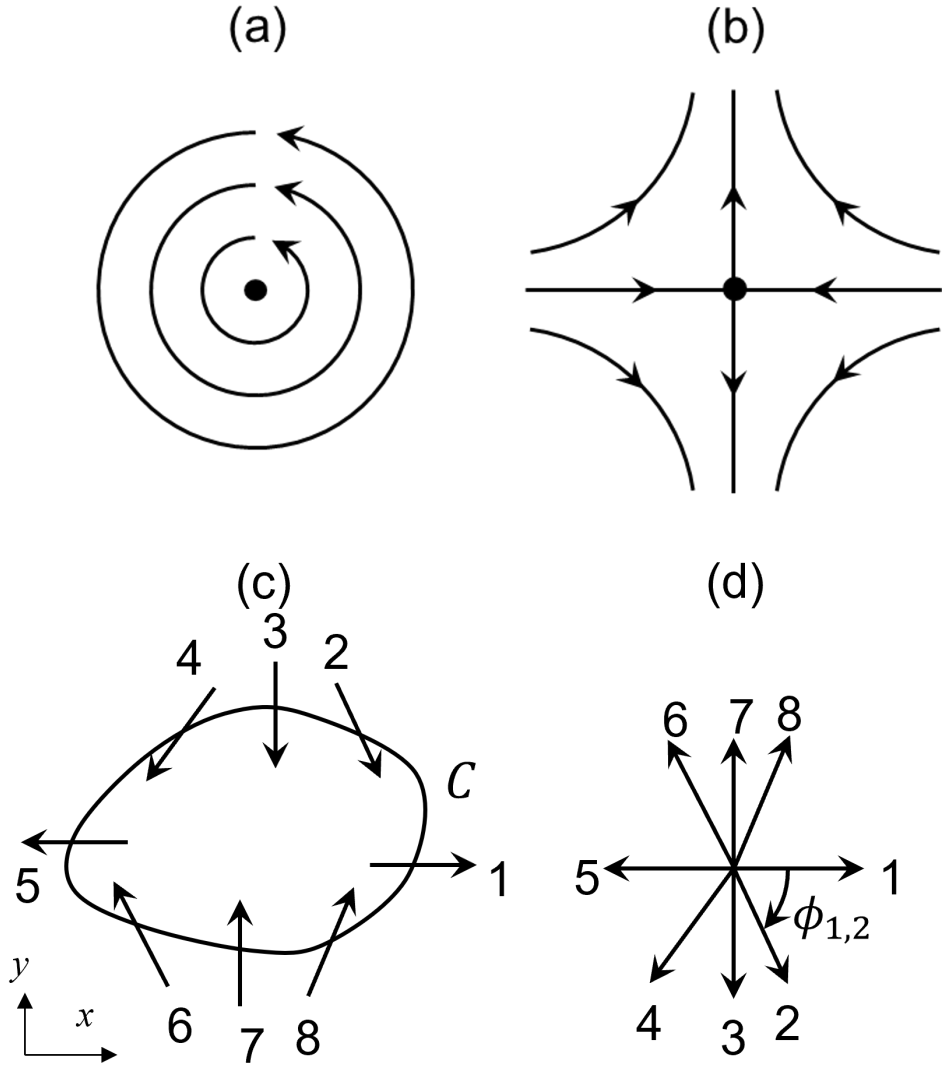

Figure 1. Schematic illustration of (a) center and (b) saddle points in vector field and (c) example of calculation of index for closed loop *C* including saddle point inside loop. $\phi_{1,2}$ represents the angle between the vectors 1 and 2. When the closed curve *C* is rotated once counterclockwise, (d) the vector rotates clockwise from 1 to 8 and the index can be calculated as -1.

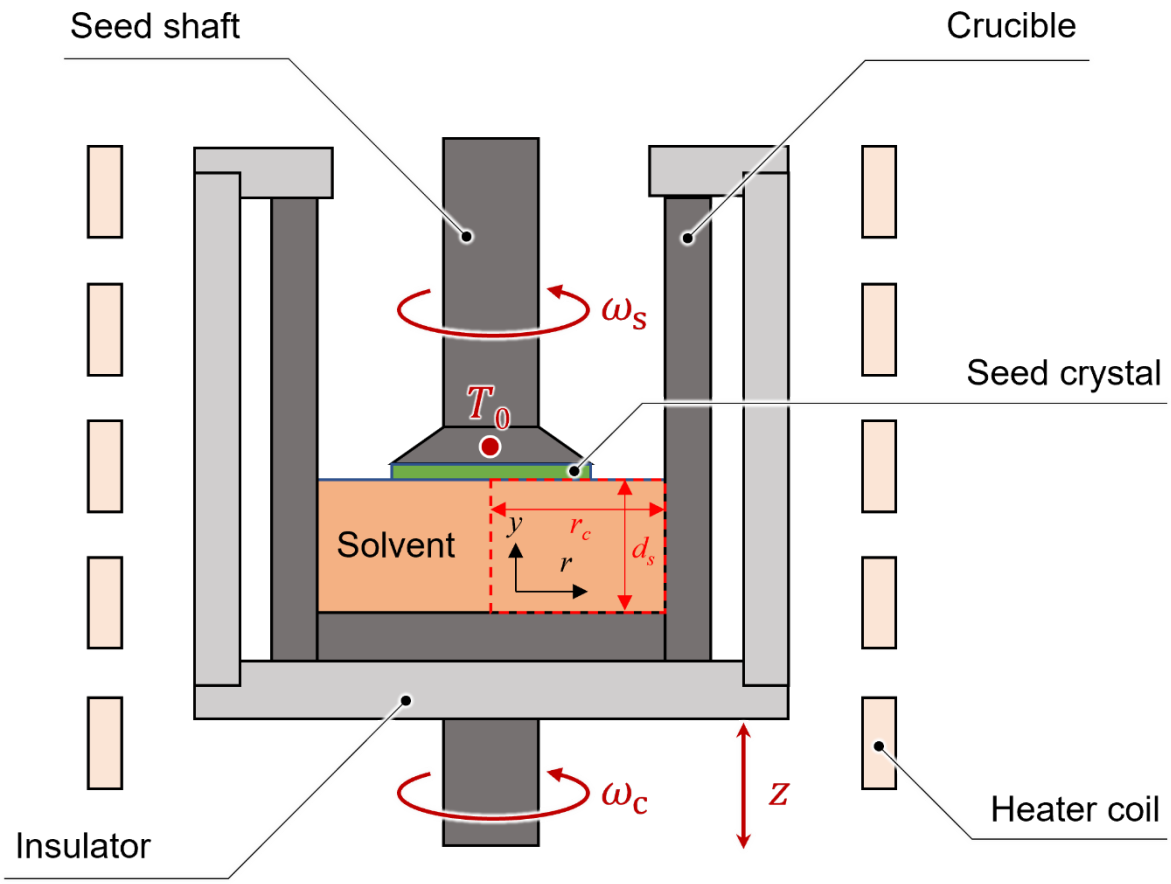

Figure 2. Schematic illustration of TSSG furnace for 6 inch.

Table 1. Ranges of variable parameters for CFD simulations.

Parameter	Symbol	Units	Lower limit	Upper limit
Rotation speed of seed crystal	ω_s	rpm	0	200
Rotation speed of crucible	ω_c	rpm	-50	50
Position of crucible	z	mm	140	200
Temperature	T_0	K	2073	2173

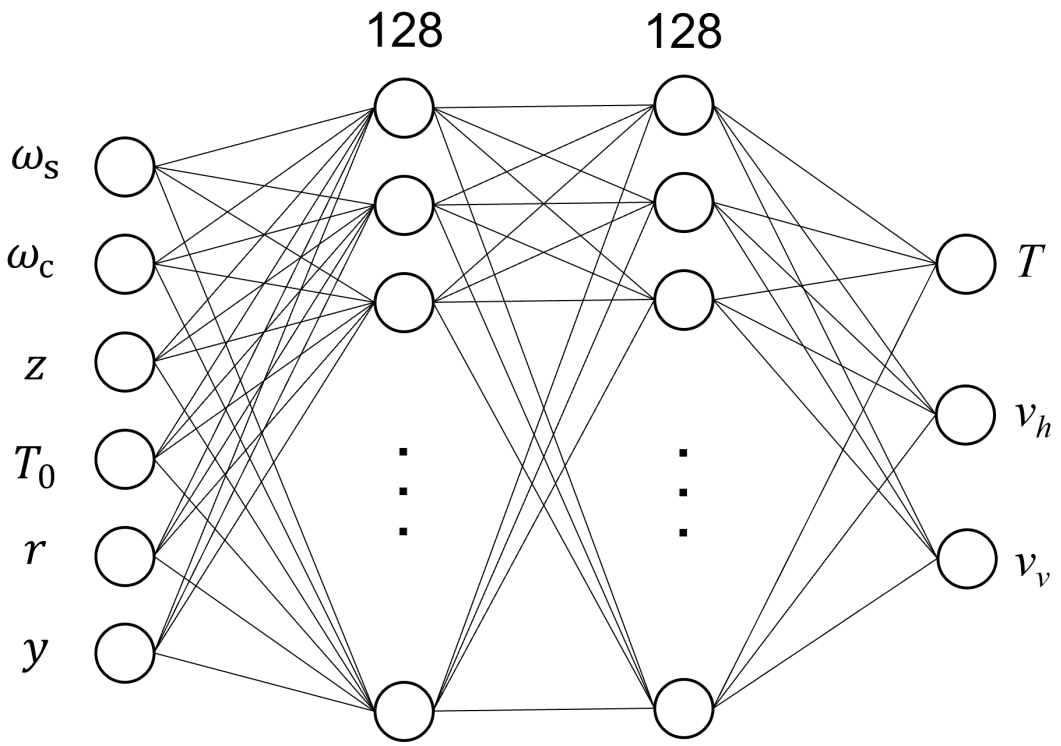

Figure 3. Structure of neural networks for prediction of temperature and solution flow distributions from variable parameters.

Table 2. Coefficients of determination (R^2) and average root mean square error (RMSE) for the prediction values of temperature, horizontal flow velocity, vertical flow velocity.

Parameter	R^2 score	RMSE
T	0.999	0.273 K
v_h	0.996	1.14 mm/s
v_v	0.996	0.593 mm/s

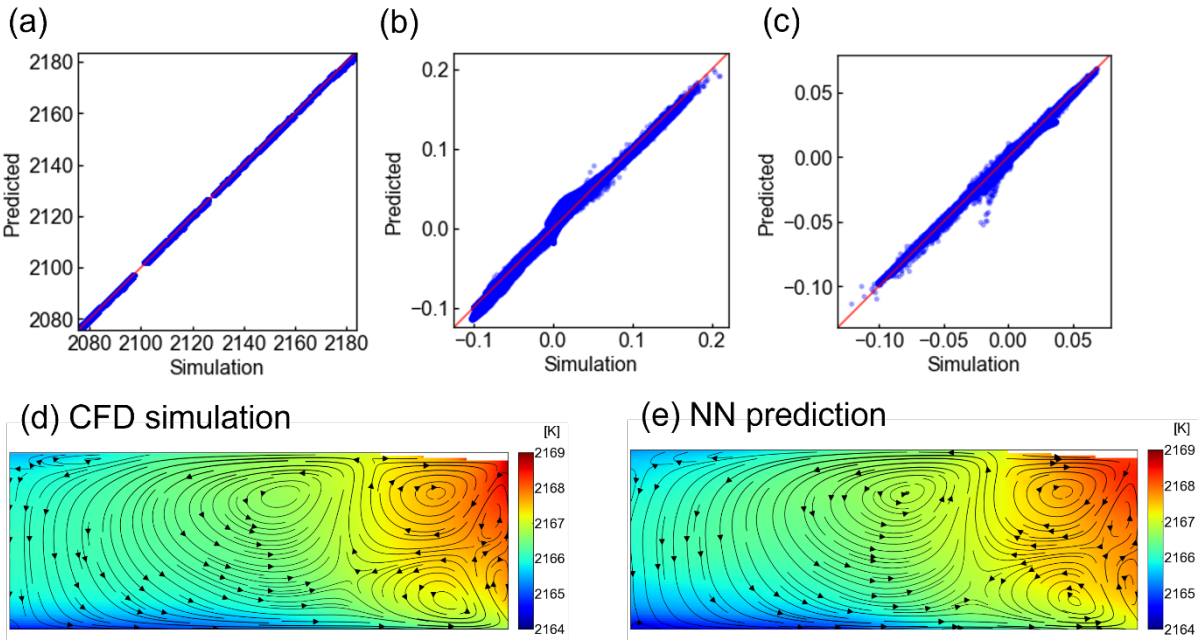

Figure 4. Parity plots of (a) the temperature (K), (b) horizontal flow velocity (m/s), and (c) vertical flow velocity (m/s) for the test data as well as (d) one example of CFD simulation and (e) corresponding predicted distributions of temperature and fluid flow for 6-inch crystal growth.

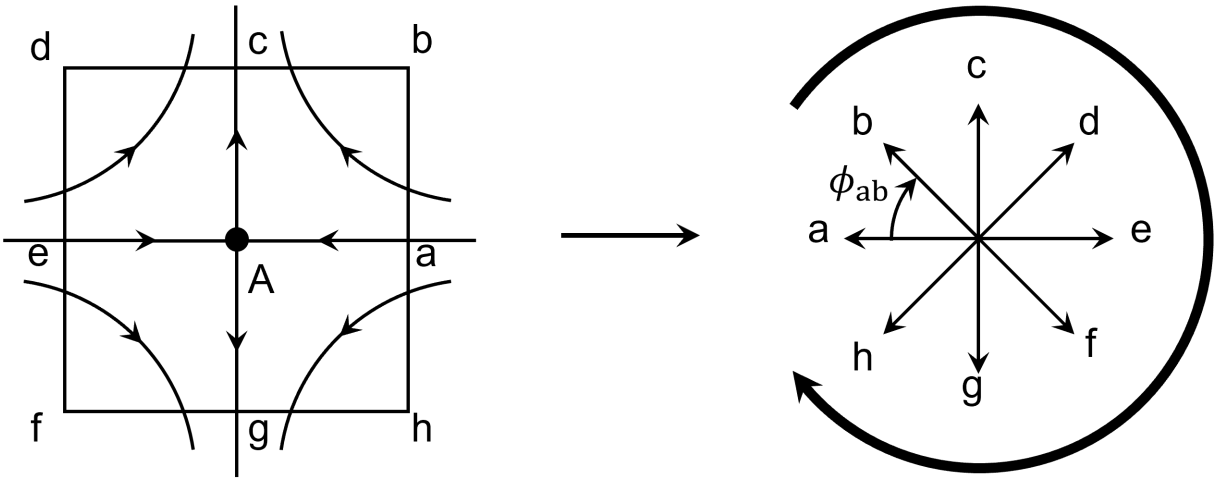

Figure 5. Schematic illustration of index calculation for flow velocity at point A. The sum of the angles between the vectors at the 8 points neighoring A (a-h) can determine whether the point A is a stagnation point or not based on index theory.

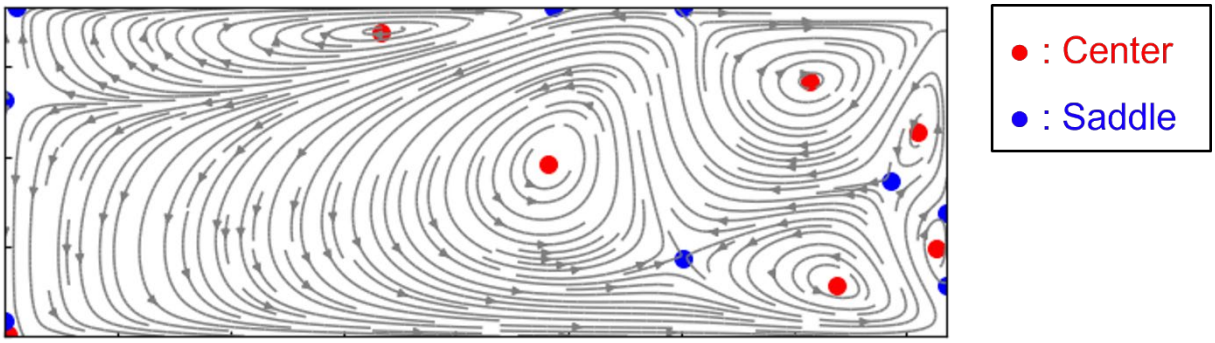

Figure 6. Example of extraction of center and saddle points in fluid flow by CFD simulation for 6-inch crystal growth. Note that this solution flow distribution was randomly picked up from the CFD simulation results for the demonstration of automatic extraction of stagnation points and was not related to the optimal solution flow distribution.

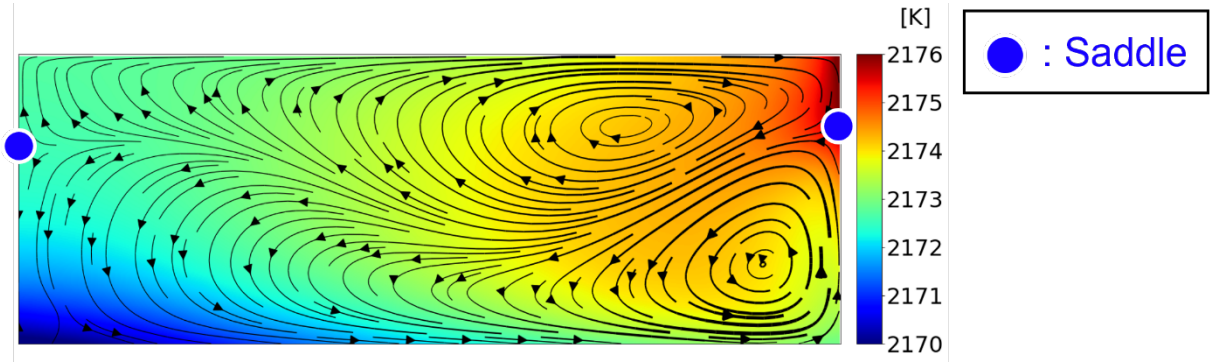

Figure 7. Empirically optimal global flow distribution in 3-inch TSSG experiment, in which two vortexes are separated at the top and bottom.

Table 3. Values of objective functions and parameters for pareto solutions.

Solution#	F_1 (K)	F_2 (m/s)	F_3 (mm)	ω_s (rpm)	ω_c (rpm)	z (mm)	T_0 (K)
(A)	1.64	0.0485	1.21	155	-42	146	2073
(B)	2.51	0.0310	16.6	80	-21	200	2073
(C)	4.22	0.00517	52.0	30	-12	153	2079
(D)	5.66	0.00828	17.1	13	9	197	2173
(E)	2.48	0.0111	-	59	-24	200	2073
(F)	3.19	0.0246	8.84	53	-12	200	2073

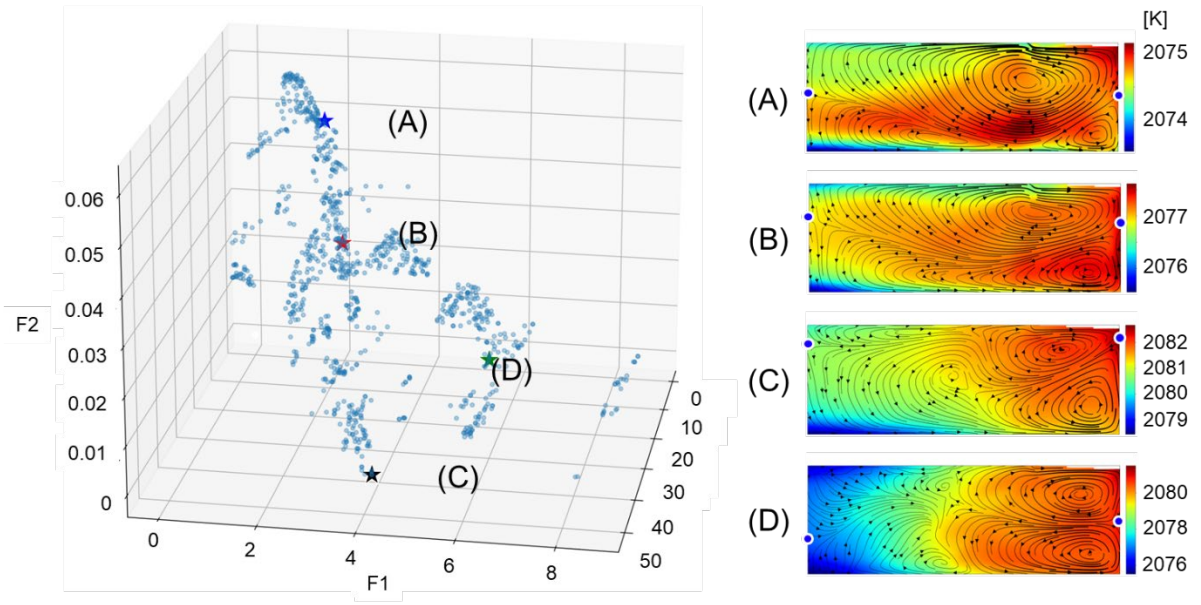

Figure 8. Pareto front for three objective functions F_1, F_2 and F_3 as well as distributions of temperature and solution flow velocity with selected optimal solutions for 6-inch crystal growth.

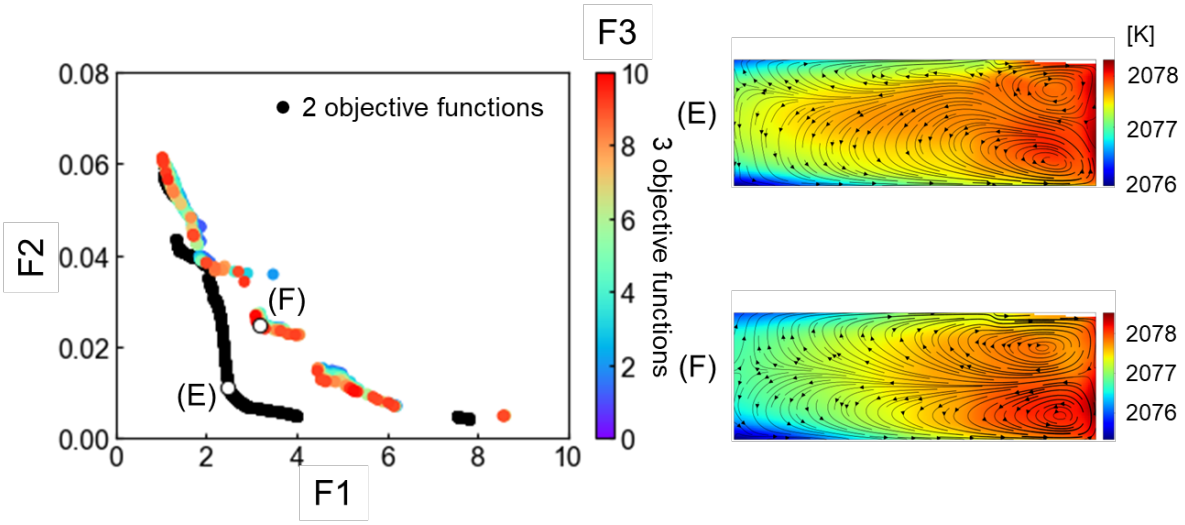

Figure 9. Pareto front for two objective functions F_1 and F_2 in comparison with three objective functions with F_3 less than 10, as well as distributions of temperature and solution flow velocity for 6-inch crystal growth with selected solutions.